

## Study of the Al coordination in mullites with varying Al:Si ratio by $^{27}\text{Al}$ NMR spectroscopy and X-ray diffraction

P. REHAK,<sup>1</sup> G. KUNATH-FANDREI,<sup>1</sup> P. LOSSO,<sup>1</sup> B. HILDMANN,<sup>2</sup> H. SCHNEIDER,<sup>2</sup> and C. JÄGER<sup>1,\*</sup>

<sup>1</sup>Friedrich-Schiller-Universität Jena, PAF, IOQ, D-07743 Jena, Germany

<sup>2</sup>Deutsche Forschungsanstalt für Luft-und Raumfahrt, Institut für Werkstoff-Forschung, Linder Höhe, D-51147 Köln, Germany

### ABSTRACT

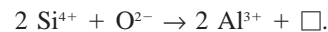
Mullite is an aluminosilicate of the composition  $\text{Al}_2(\text{Al}_{2+2x}\text{Si}_{2-2x})\text{O}_{10-x}$  with  $x$  generally ranging between 0.2 and 0.5. XRD and  $^{29}\text{Si}$  and  $^{27}\text{Al}$  nuclear magnetic resonance (NMR) have been used to investigate the structure of various mullite compositions ( $x = 0.26, 0.36, 0.42,$  and  $0.69$ ) as well as sillimanite ( $x = 0$ ) and  $\gamma\text{-Al}_2\text{O}_3$  ( $x = 1$ ).  $^{27}\text{Al}$  magic angle spinning (MAS) NMR of the central and satellite transitions have been used to determine the chemical shifts and quadrupole interaction parameters for the various  $\text{AlO}_4$  and  $\text{AlO}_6$  units. The isotropic chemical shifts of the various units are 5.9 ppm for  $\text{AlO}_6$ , 69.1 ppm for  $\text{AlO}_4(\text{T})$ , 55.0 ppm for  $\text{AlO}_4(\text{T}')$ , and 45.7 ppm for  $\text{AlO}_4(\text{T}^*)$  where  $\text{AlO}_4(\text{T})$  denotes the aluminum tetrahedra in the double chains, and  $\text{AlO}_4(\text{T}')$  and  $\text{AlO}_4(\text{T}^*)$  those next to the oxygen  $\text{Oc}^*$ . Quantitative numbers of the aluminum occupancy of these sites have been determined for the various powder samples. These results are in good agreement with the average structure model of mullites. NMR and XRD proved the presence of impurities of kyanite in natural sillimanite and of  $\gamma\text{-Al}_2\text{O}_3$  in the mullites with  $x = 0.42$  and  $0.69$ .

### INTRODUCTION

Mullite is an important ceramic material for both traditional and advanced applications. The material is characterized by a very good thermal stability especially under oxidizing conditions. Furthermore, mullite materials have a low thermal expansion coefficient and very low thermal conductivity combined with excellent creep resistance (Somiya et al. 1990; Davies et al. 1990; Schneider et al. 1994b). The mullite formation has been extensively investigated using various routes, e.g., thermal decomposition of kaolinite (e.g., Brindley and Nakahira 1959a, 1959b, 1959c; Boch et al. 1990; for further reference see also Schneider et al. 1994a), reaction sintering of the oxides (Schmücker et al. 1994; Boch et al. 1990; Sanz et al. 1988, see also Schneider et al. 1994a), spray pyrolysis (Sanz et al. 1991) and by various sol-gel routes (e.g., Taylor and Holland 1993; Schneider et al. 1992, 1994b). There is also a crystallochemical interest on mullite, on non-crystalline gels (mullite precursors), and glasses with mullite composition.

Mullite is a member of the aluminum silicates of the composition  $\text{Al}_2(\text{Al}_{2+2x}\text{Si}_{2-2x})\text{O}_{10-x}$  with  $x$  generally ranging between 0.2 and 0.5 (Cameron 1977a, 1977b). Recent investigations on sol-gel produced mullites have shown that extremely  $\text{Al}_2\text{O}_3$ -rich mullites ( $x > 0.8$ ) also can be formed (Schneider et al. 1993; Fischer et al. 1994). Under normal stable conditions two mullite compositions have been described, so-called 3/2-mullites with about 72 wt%  $\text{Al}_2\text{O}_3$  ( $x \approx 0.25$ ) and 2/1-mullite with about 77 wt%

$\text{Al}_2\text{O}_3$  ( $x \approx 0.4$ ). The average structure of 3/2-mullite was determined by Saalfeld and Guse (1981), that of 2/1-mullite by Burnham (1963, 1964a, 1964b), Durovic (1969), and Angel and Prewitt (1986). The mullite structure consists of chains of edge-sharing  $\text{AlO}_6$  octahedra running parallel to the crystallographic  $c$  axis similar to those of sillimanite (Fig. 1a) (Bish and Burnham 1992; Sadanaga et al. 1962). The octahedral chains are crosslinked by double chains of  $(\text{Al},\text{Si})\text{O}_4$  tetrahedra [denoted as  $\text{AlO}_4(\text{T})$  for aluminum in Fig. 1b]. The substitution of Si by Al in mullite produces O vacancies  $\square$  and the formation of  $\text{AlO}_4$  tetrahedra triclusters [ $\text{AlO}_4(\text{T}^*)$  and  $\text{AlO}_4(\text{T}')$  in Fig. 1, explanations further below] sharing a common O atom  $\text{Oc}^*$  according to:



We explicitly note that those tetrahedra around  $\text{Oc}^*$  have been assigned to as  $\text{AlO}_4(\text{T}^{\text{s}})$  by Sadanaga (additional superscript S for Sadanaga) because  $\text{AlO}_4(\text{T}^*)$  and  $\text{AlO}_4(\text{T}')$  could not be distinguished by X-ray diffraction (XRD). Comprehensive studies of the structure have been performed using sophisticated spectroscopic techniques (e.g., Rager et al. 1990; Bauchspiess 1995, see also Schneider et al. 1994a), X-ray or neutron diffractometry, and transmission electron microscopy (TEM; Angel et al. 1991; Rahman and Weichert 1990).  $^{27}\text{Al}$  MAS NMR is useful for probing the existence of four-, five- and six-fold-coordinated Al species during the mullite formation and in glasses and gels of the  $\text{Al}_2\text{O}_3\text{-SiO}_2$  system (Albers 1993; Sanz et al. 1988, 1991; Taylor and Holland 1993; Schneider et al. 1992; Merwin et al. 1991) although it is

\* E-mail: p6jach@physik.uni-jena.de

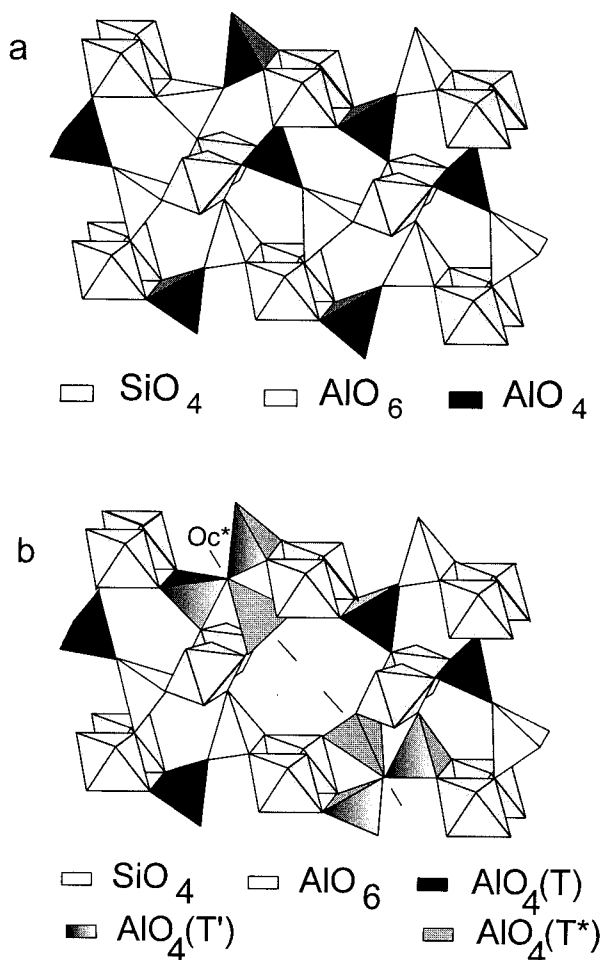


FIGURE 1. Framework of the connected Al and Si coordination polyhedra of sillimanite (a) and mullite (b). For details see text.

difficult to obtain reliable quantitative numbers of the relative amount of Al in the various O polyhedra. This also applies for the quantitative determination of four- and six-fold-coordinated Al in mullites, where the standard <sup>27</sup>Al MAS NMR signal of the so-called central transition CT ( $m = 1/2 \leftrightarrow m = -1/2$ ) yields only qualitative results for Al in the T and T\* sites (Angel et al. 1991).

Recently, <sup>27</sup>Al NMR satellite transition (ST) spectroscopy has been used for a quantitative study of the Al distribution of polycrystalline 2/1-type mullite ( $\approx 76$  wt% Al<sub>2</sub>O<sub>3</sub> and  $\approx 24$  wt% SiO<sub>2</sub>) (Kunath-Fandrei et al. 1994a). Using the improved resolution of the <sup>27</sup>Al MAS spinning sidebands of the inner ST's (Samoson 1985) three different AlO<sub>4</sub> units were found at isotropic chemical shifts of 68, 53, and 45 ppm. These resonances were assigned to as AlO<sub>4</sub> units in the tetrahedral double chains [AlO<sub>4</sub>(T)] and the two types of tricluster tetrahedra AlO<sub>4</sub>(T') and AlO<sub>4</sub>(T\*), respectively (cf. Fig. 1b), that could be distinguished for the first time.

The present study focuses particularly on the quanti-

tative determination of the Al occupancy of the various AlO<sub>n</sub> units ( $n = 4, 6$ ) for polycrystalline mullite samples with varying Si/Al ratios, including a natural sillimanite ( $x = 0$ ) sample and  $\gamma$ -Al<sub>2</sub>O<sub>3</sub> ( $x = 1$ ) as reference materials. The results are discussed in terms of the average structure model for mullites.

## EXPERIMENTAL METHODS

### Sample preparation

**Sample FM.** The 2/1 mullite material was produced in a commercial electric arc furnace by casting a melt of Al<sub>2</sub>O<sub>3</sub> and kaolinite in a mold at  $T > 2000$  °C, followed by a temperature-controlled cooling and recrystallization process. According to electron microprobe analysis the chemical composition of the mullite is typically: Al<sub>2</sub>O<sub>3</sub> = 75.9(8) wt% and SiO<sub>2</sub> = 23.8(5) wt% (numbers in parentheses are standard deviations; number of analysis is 14). The chemical analyses and the determination of the lattice constants show that the mullite composition is close to that of the 2/1-type ( $x \approx 0.36$ ).

**Sample CM1.** Tetraethoxysilane (TEOS) was first diluted with isopropanol (1:1) and then prehydrolyzed with H<sub>2</sub>O (26 mole H<sub>2</sub>O/mole TEOS). This solution was admixed with a solution of aluminum-sec-butylate [Al(OBu<sup>s</sup>)<sub>3</sub>] and isopropanol (1:1), which caused rapid gel formation. The dried gel (150 °C) was heat-treated at 1600 °C for 15 h. The reaction product corresponds to a mullite with stoichiometric mullite composition ( $\approx 72$  wt% Al<sub>2</sub>O<sub>3</sub>, 28 wt% SiO<sub>2</sub>).

**Sample CM2.** TEOS was diluted in equal volumes isopropanol, and prehydrolyzed with H<sub>2</sub>O (10 min, 1:1). Afterward it was mixed with in equal volumes isopropanol diluted [Al(OBu<sup>s</sup>)<sub>3</sub>] in the same proportions as for sample CM1. After stirring the admixture for 2 h the hydrolysis took place by air contact in petri dishes ( $T = 20$  °C, relative humidity = 40%) in a glove box over several days. This prepared gel was dried at 150 °C for 15 h and heat treated at 950 °C for 15 h. The sample corresponds to the type I precursor (Schneider et al. 1993).

**Sample CM3.** Precursor CM3 was prepared by mixing the reagents aluminum-sec-butylate [Al(OBu<sup>s</sup>)<sub>3</sub>] and silicon tetrachloride SiCl<sub>4</sub> without solvent in air ( $T = 24$  °C) in proportions corresponding to an Al/Si ratio of 4/1. After 5 min of homogenization, a low amount of deionized water was rapidly added to the mixture. The addition of water led to a vigorous reaction with formation of a non-transparent white gel. The gel was dried at 150 °C for 15 h, crushed to powder and then heat treated at 950 °C for 2 h. The sample corresponds to supertype I precursor (Voll 1995).

**Sample SIL.** A natural mineral sample from Williams-town (Australia) was used. The sample consists of sillimanite as major and kyanite as minor phase, in addition to an unknown alumina containing impurity phase.

**Sample GAM.** Chemically pure AlOOH (Pural SCF, Condea Chemie) was used as starting material. By heat treatment at 550 °C (15 h) it transforms completely into  $\gamma$ -Al<sub>2</sub>O<sub>3</sub>.

The compositions of all samples were determined from the lattice parameters using XRD. This is described in detail in the Results section.

### Nuclear magnetic resonance

The observation of the MAS spinning sidebands of the inner ST ( $m = \pm 3/2 \leftrightarrow m = \pm 1/2$ ) has been used by several groups to study the quadrupole interaction in solids (e.g., Alemany et al. 1991; Skibstedt et al. 1991). However, for any  $I = 5/2$  nucleus such as  $^{27}\text{Al}$  the 2<sup>nd</sup> order quadrupolar broadening is reduced by a factor of about three simply by a lucky combination of the nuclear spin number  $I$  and the NMR transition  $m$  (Samoson 1985). We have used this improved resolution to study the structure of solids (Jäger et al. 1992, 1993a, 1993b; Kunath et al. 1992; Kunath-Fandrei et al. 1994a, 1994b, 1995a, 1995b; Smith et al. 1994). Particularly, in disordered samples the quadrupole broadening of these ST-spinning sidebands is often suppressed to such a degree that a limit of spectral resolution is achieved that is governed by isotropic chemical shift distributions.

The correct acquisition of the complete ST MAS spectrum is a major problem because a large frequency range of a few kilohertz up to several megahertz must be recorded. We use an approach (Jäger 1994), where two or even more spectra are acquired. One experiment is carried out setting the rf irradiation exactly at the CT, whereas the other spectra are acquired with several frequency offsets (e.g., 400 kHz, 800 kHz, 1.2 MHz) and carefully retuned probe. These spectra must be corrected afterward for the frequency characteristics of the probe (LC circuit) including the finite pulse width effects as outlined previously (Jäger 1994). Finally, these on- and off-resonance spectra are combined to give the complete ST MAS spectrum. Details of the spectra simulations including distributions of the quadrupole interactions can be found elsewhere (Skibstedt et al. 1991; Jäger et al. 1993a).

The  $^{27}\text{Al}$  NMR spectra were measured using a BRUKER ASX 500 spectrometer operating at 130.32 MHz and a BRUKER 4 mm MAS probe. Extremely short pulses (1.0  $\mu\text{s}$ ) were used being equivalent to a pulse angle of about 15° necessary for a correct quantitative determination of the Al occupancy for sites with different quadrupole coupling constants (Freude and Haase 1993). The repetition time was 1.3 s and no saturation effects were observed. About 7000 scans were accumulated with a spinning frequency of 14 kHz. The MAS frequency was stable to within 2 Hz. The sweep width was set to 2.5 MHz. Data points of 16 k were acquired and zero filled to 64 k prior to the Fourier transform. The severe baseline problems due to deadtime and finite pulse width have been removed by cubic spline baseline correction mode provided by the spectrometer software. An on-resonance and an off-resonance experiment at 500 kHz were acquired and used to obtain the complete ST MAS spectra.

Most of the CT MAS spectra are broadened by distributions of the electric field gradients (efg). In an earlier paper (Jäger et al. 1993a) we described both the model

and the resulting NMR spectra. As the principal axes values of the efg tensor are distributed in that model (mean value and Gaussian-like distribution) we express these principal axis values in terms of the corresponding quadrupole frequency. This procedure makes (although somewhat artificially) the size of the efg values more clear.

### X-ray diffractometry

The XRD measurements were performed on the oxide samples mixed with powdered pure silicon as an internal standard. Flat silicon sample holders were used to reduce scattering background intensity. These sample holders were cut from a single crystal such that no Si reflection appeared over the whole 2 $\theta$  scan region. Data collections were performed with a computer-controlled Siemens D 5000 diffractometer, equipped with a graphite monochromator in front of the scintillation counter. Diffraction patterns were recorded at room temperature with  $\text{CuK}\alpha$  radiation in the 2 $\theta$  range between 14 and 90°, at 40 kV and 40 mA. Step scans were acquired in increments of 0.01° and intervals of 4 s. The receiving slit was 0.2 mm and the divergence slit was an ADS type.

For the evaluation of 2 $\theta$  peak positions the program module FIT (Siemens, DIFFRAC-AT V 3.3) was used. The background was taken into account by linear interpolations underneath groups of up to seven reflections, which were fitted simultaneously. The profile function SPLIT P7 was best suited for the simulation of the peak shape with two refinable common exponents  $s$  and  $t$  for the Lorentzian profile type. The 2 $\theta$  positions of the fitted  $\text{CuK}\alpha_1$  profiles were used in subsequent calculations. The observed mullite positions were corrected using the internal standard Si reflections. The differences between observed and calculated silicon peak positions [ $\Delta 2\theta = 2\theta_o - 2\theta_c$ ,  $a(\text{Si}) = 5.43102 \text{ \AA}$ ,  $\lambda = 1.54057 \text{ \AA}$ ] were fitted by functions of the type  $\Delta 2\theta = A_0 + A_1 \sin(2\theta) + A_2 \cos(\theta)$  representing corrections due to zero point shifts, absorption effects [ $\sim \sin(2\theta)$ ], and eccentricity of sample surface in normal direction [ $\sim \cos(\theta)$ ]. Least-square refinements of the lattice parameters were performed using a standard program module (LCLSQ).

## RESULTS

### XRD characterization

The XRD patterns of the mullites SM-O and CM1 have narrow reflection peaks due to a high crystallinity. In contrast, the XRD patterns of the sol-gel prepared samples CM2 and CM3 exhibit considerably broadened reflection profiles, indicating non-perfect crystallinity. Sample CM3 exhibits a noticeable amount of  $\gamma\text{-Al}_2\text{O}_3$ . The measured lattice parameters  $a$ ,  $b$ ,  $c$ , and  $V$  are summarized in Table 1 and plotted in Figure 2 together with values from the literature used as calibration data. Several authors (e.g., Cameron 1977a, 1977b; Klug et al. 1990; Ban and Okada 1992; Schneider et al. 1993; and Fischer et al. 1994) have shown that the chemical composition of the mullite phase can be obtained from a linear relationship between the lattice parameter  $a$  and the molar  $\text{Al}_2\text{O}_3$  content  $m$ . Using

TABLE 1. XRD results

Samples	$N_{\text{obs}}$	$a$	$b$	$c$	$V$	$m$	$x$	
SIL	32	7.4850(3)	7.6736(3)	5.7710(3)	331.462(12)	50.36	0.010	
CM1	35	7.5460(1)	7.6919(1)	2.8843(1)	167.412(3)	60.37	0.259	
FM	30	7.5759(3)	7.6871(2)	2.8862(1)	168.080(7)	64.78	0.359	
CM2	16	7.5989(12)	7.6936(12)	2.8813(3)	168.448(30)	67.70	0.422	
CM3	12	7.6821(31)	7.6414(31)	2.9069(6)	170.643(75)	81.04	0.686	
Calibration samples, Ref.		Methods						
Pittipanny, Guse (1979)		SC-diff, MP	7.4810(10)	7.6700(10)	5.7730(10)	331.250(42)	49.63	-0.010
Norwich, JCPDS-38-471		P-diff, CA	7.4860(10)	7.6750(10)	5.7729(6)	331.682(36)	50.56	0.015
SM-O, Schneider (1990)		Guinier, MP	7.5440(4)	7.6896(4)	2.8837(2)	167.285(11)	59.47	0.237
SM-O, this work		P-diff, $N_{\text{obs}} = 52$	7.5432(2)	7.6902(3)	2.8840(1)	167.295(7)	59.47	0.237
FM (brick), Schneider (1993)		Bond, MP	7.58045	7.68227	2.88534	168.028	65.23	0.369
FM-O (CZ), Schneider (1990)		Guinier, MP	7.5823(6)	7.6819(5)	2.8865(2)	168.130(13)	65.99	0.385
FSS, Fischer (1994)		P-diff, ATEM	7.7391(6)	7.6108(5)	2.9180(1)	171.872(13)	89.00	0.825
$\iota$ -Al <sub>2</sub> O <sub>3</sub> , this work		$a \sim M$ , $V \sim m$ extrapolation	7.809	7.552	2.943	173.559	100.0	1.000

Note: Refined lattice parameters  $a$ ,  $b$ ,  $c$  (Å) and  $V$  (Å<sup>3</sup>) of the NMR samples together with values from the literature used for calibrating the relationships between lattice parameters and the molar content of Al<sub>2</sub>O<sub>3</sub>.  $N_{\text{obs}}$  represents the number of reflections included in the least squares refinements. Least squares standard deviations are given in parentheses and refer to the last digits. SC-diff: single crystal diffractometry, P-diff: powder diffractometry, Guinier: Guinier film method, Bond: high resolution single crystal diffractometry with Bond's method, MP: microprobe analyses, CA: chemical analyses, ATEM: analytical transmission electron microscopy. The diffraction pattern of sample FSS was refined by Rietveld's method. In all cited X-ray measurements on powdered samples Si was used as an internal standard, as also done in the present study.

the data of sillimanite, mullite lattice parameters, and compositions from the given references in Table 1, it becomes evident that a linear relationship between the volume of the unit cell  $V$  and the molar alumina content  $m$  holds true as well (cf. Fig. 2). In addition, linear regressions yield straight lines for  $a \sim m$  and  $V \sim m$  including the sillimanite composition:

$$a [\text{Å}] = 0.00655(8) * m [\text{mol\% Al}_2\text{O}_3] + 7.1538(50) [\text{Å}]$$

$$V [\text{Å}^3] = 0.1571(25) * m [\text{mol\% Al}_2\text{O}_3] + 157.85(16) [\text{Å}^3].$$

Standard deviations for the values of the intercepts and slopes are given in parentheses resulting from the least-square calculations. The linear relationship between  $V$  and  $m$ , in addition to the well-established correlation between  $a$  and  $m$  for mullite mixed crystals, was heretofore unrecognized. The equation  $a \approx m$  obtained in this study agrees well with that published by Fischer et al. (1996)  $a [\text{Å}] = 0.00692(8) * m [\text{mol\% Al}_2\text{O}_3] + 7.1240(50) [\text{Å}]$  in the Al-rich region, but deviates in the sillimanite region.

The calibration sample SM-O was measured a second time (referred to as "this work" in Table 1) to test the experimental accuracy. A good agreement between the two sets of obtained lattice parameters is found (see Table 1). The two sillimanite calibration samples, natural minerals from the U.S.A., contain small amounts of Fe<sub>2</sub>O<sub>3</sub> impurities corresponding to 0.42 and 0.91 mol% Fe<sub>2</sub>O<sub>3</sub>, respectively. These molar Fe<sub>2</sub>O<sub>3</sub> contents were added to the molar Al<sub>2</sub>O<sub>3</sub> content, because Fe is incorporated on octahedral sites in the sillimanite structure, which leads likewise to an increase of  $a$  and  $V$  as Al does. Up to now, a pure sillimanite sample as reference material was not available. The molar content  $m$  of the NMR samples and the value  $x$  given in Table 1 were obtained from our cal-

ibration curves  $a \approx m$  and  $V \approx m$  given above. The mean value from both given correlations was taken.

The non-linear relationships between the lattice parameters  $b$  and  $c$  and the molar Al<sub>2</sub>O<sub>3</sub> content  $m$  can be approximated by polynomial regressions of 3<sup>rd</sup> order (cf. Fig. 2) reasonably well. Assuming that both relations persist up to the ultimate Al<sub>2</sub>O<sub>3</sub> contents of mullite, the lattice parameter of  $\iota$ -Al<sub>2</sub>O<sub>3</sub>, with a hypothetical mullite structure type, can be determined by extrapolation: linear regressions for  $a$  and  $V$ , and polynomial regressions for  $b$  and  $c$ , taking into account the boundary condition  $V/a = b * c$ . These theoretical values are added to Table 1, and the extrapolations are shown in Figure 2 as dotted lines.

#### <sup>27</sup>Al NMR satellite transition spectroscopy

The <sup>27</sup>Al CT MAS patterns of the various mullites (Fig. 3a, spectra B–E) are similar to those reported earlier (Sanz et al. 1991; Schneider et al. 1992; Merwin et al. 1991). The spectra consist of a line with a peak position at about 0.5 ppm (AlO<sub>6</sub> octahedra) and a second broad resonance (AlO<sub>4</sub> tetrahedra) with more or less resolved peaks at about 44 and 59 ppm. The various resonances of the AlO<sub>4</sub> sites overlap partially, making a quantitative analysis of the CT MAS pattern difficult. Both resonance lines are strongly asymmetric due to the distributions of the main axes values of the efg tensor although the material is crystalline. Similar conclusions apply for the MAS line shape of  $\gamma$ -Al<sub>2</sub>O<sub>3</sub> (Fig. 3, spectrum F). In contrast, the <sup>27</sup>Al MAS spectrum of sillimanite shows several singularities and shoulders as to be expected for polycrystalline samples not having distributions of the quadrupole interaction. Additionally, a few weak MAS sidebands are shown in Figure 3a for each of the samples. They belong to the inner ST, and the complete left half of the ST MAS line shape of the mullite CM1 is shown

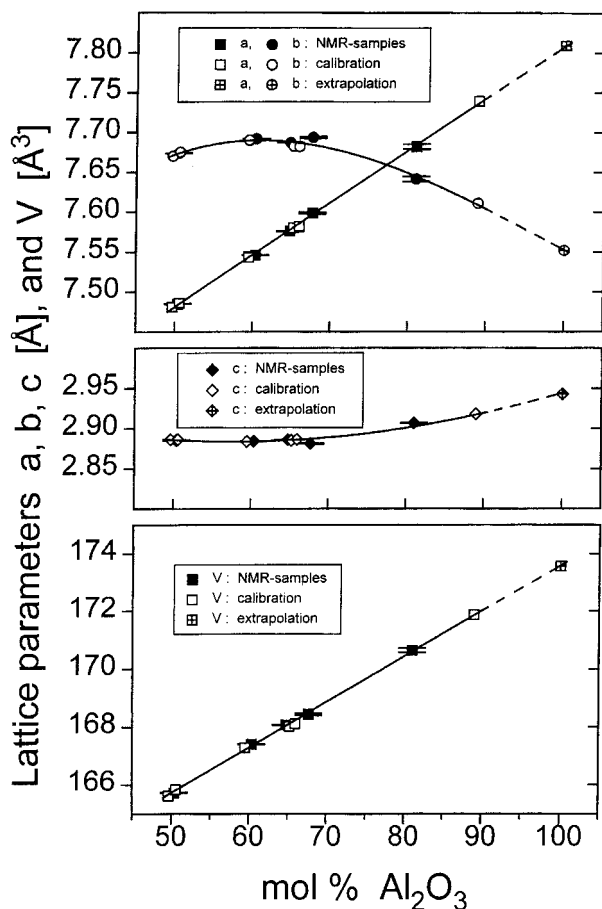


FIGURE 2. Lattice parameters  $a$ ,  $b$ ,  $c$ , and  $V$  vs. Al<sub>2</sub>O<sub>3</sub> contents. Because of the disordered Si/Al distribution in the (Al,Si)O<sub>4</sub> tetrahedra in mullite the lattice constant  $c_{\text{mull}}$  has a repeat of about 2.9 Å, half of that of sillimanite. Therefore,  $c_{\text{sil}}/2$  and  $V_{\text{sil}}/2$  are plotted for sillimanite. Dotted lines represent extrapolations to mullite with 100 mol% Al<sub>2</sub>O<sub>3</sub> content ( $\gamma$ -Al<sub>2</sub>O<sub>3</sub>).

in Figure 3b for comparison. Note the large frequency range that covers more than 1 MHz or more than 8000 ppm compared to only about 200 ppm for the CT MAS spectra. It is clear that the quadrupole parameters of the AlO<sub>6</sub> and AlO<sub>4</sub> resonance differ slightly because the envelope of the ST MAS sidebands is different.

In Figure 4 a few of these ST MAS spinning sidebands are plotted in the same order as the corresponding CT MAS spectra of Figure 3. Due to the improved spectral resolution AlO<sub>4</sub> (single star) and AlO<sub>6</sub> (double star) signals are completely resolved. Furthermore, the AlO<sub>6</sub> lines of the mullites and  $\gamma$ -Al<sub>2</sub>O<sub>3</sub> are almost symmetric, which means that the remaining 2<sup>nd</sup> order broadening is obviously negligible compared with the chemical shift effects. Also, for the Al-rich mullites (Fig. 4, spectra D and E) a shoulder is found on the left side of the AlO<sub>6</sub> resonance. This shoulder is very pronounced for the mullite CM3 and appears at the same chemical shift as the AlO<sub>6</sub> signal of  $\gamma$ -Al<sub>2</sub>O<sub>3</sub>.

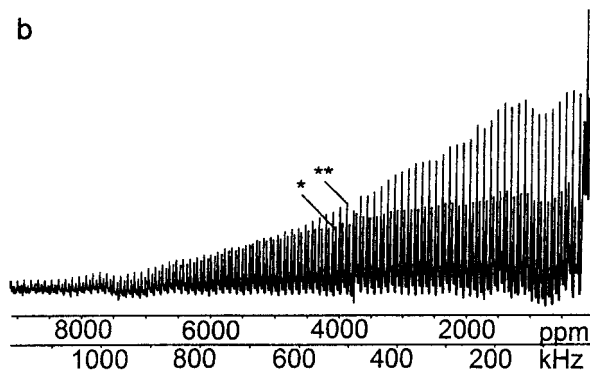
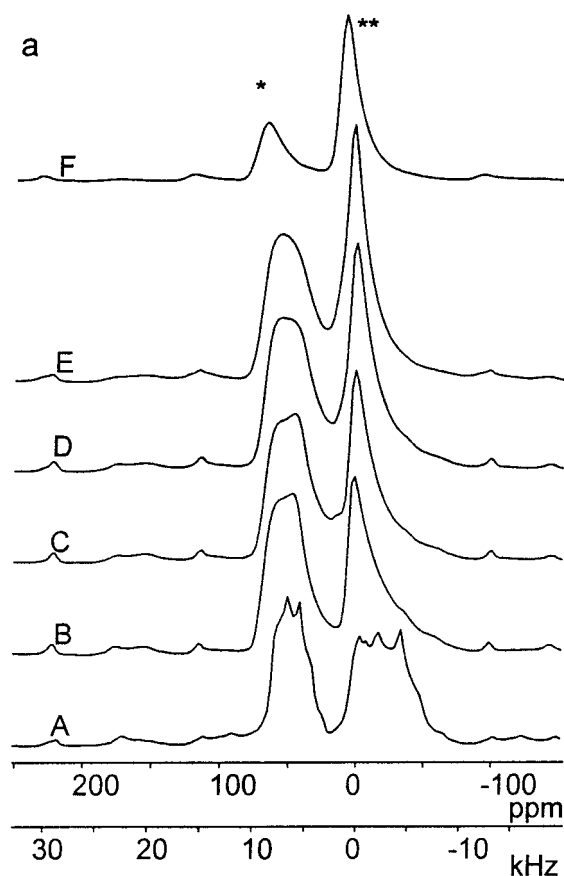


FIGURE 3. (a) <sup>27</sup>Al CT MAS spectra of the sample SIL (sillimanite) (A) and the mullite samples CM1 (B), FM (C), CM2 (D), CM3 (E) and the sample GAM ( $\gamma$ -Al<sub>2</sub>O<sub>3</sub>) (F). (b) Left half of the ST MAS spinning sidebands of mullite CM1 extending over more than 1MHz. The single and double stars indicate tetrahedrally and octahedrally coordinated Al species, respectively.

## DISCUSSION

### <sup>27</sup>Al line shape analyses and Al occupancy of the sites

In the natural sillimanite sample, kyanite was detected as an impurity both by XRD and <sup>29</sup>Si MAS NMR (spectra not shown). The known quadrupole parameters and chemical shifts for kyanite (Alemany et al. 1991; Smith

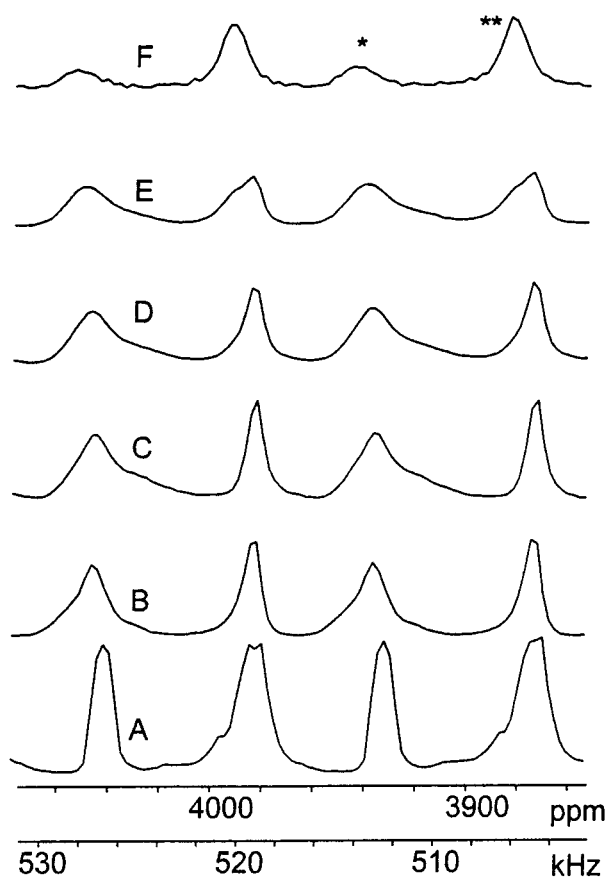


FIGURE 4. Plot of a few ST MAS spinning sidebands of SIL (sillimanite) (A) and the mullite samples CM1 (B), FM (C), CM2 (D), CM3 (E), and the sample GAM ( $\gamma$ - $\text{Al}_2\text{O}_3$ ) (F). Single star =  $\text{AlO}_4$  signal. Double star =  $\text{AlO}_6$  signal.

et al. 1994) were used for a fit of the  $^{27}\text{Al}$  CT MAS line shape of the sillimanite spectrum as the impurity kyanite contains about  $(18 \pm 2)\%$  of the total Al. The experimental and theoretical  $^{27}\text{Al}$  CT NMR line shapes are plotted in Figure 5 as top and bottom spectra, respectively. The quadrupole frequencies  $\nu_Q$  and chemical shifts  $\delta_{\text{iso}}$  are  $(1.34 \pm 0.05)$  MHz and  $(6 \pm 1)$  ppm for the  $\text{AlO}_6$  and  $(1.02 \pm 0.05)$  MHz and  $(62 \pm 2)$  ppm the  $\text{AlO}_4$  sites of sillimanite. They agree well with reported quadrupole coupling constants ( $C_Q = 20/3 \cdot \nu_Q$ ) in the literature (Lippmaa et al. 1986; Raymond and Hafner 1970; Smith 1993; Freude and Haase 1994). The relative Al occupancy for both polyhedra is 1:1 as to be expected [ $(41 \pm 2)\%$  of the total Al content for each site].

The  $^{27}\text{Al}$  MAS spectrum for  $\gamma$ - $\text{Al}_2\text{O}_3$  (GAM) must be treated differently because of the large efg distributions causing the strongly asymmetric CT MAS line shapes (Fig. 3, spectrum F) for the  $\text{AlO}_4$  and  $\text{AlO}_6$  resonances. The mean quadrupole interaction and its distribution widths for each site have been obtained from the ST MAS spinning sideband patterns that show a continuous decrease of the intensities. The quadrupole parameters and the chemical shifts are summarized in Table 2. The ex-

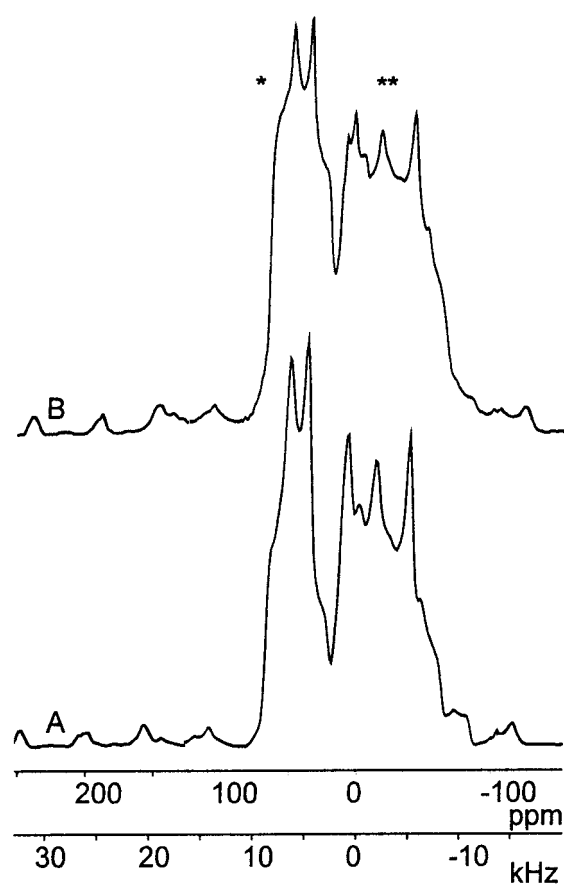


FIGURE 5. Comparison between the experimental (B) and simulated (A)  $^{27}\text{Al}$  CT MAS line shapes of the sample SIL (sillimanite). The line shape of this natural sillimanite can only be explained taking into account the kyanite spectrum besides the  $\text{AlO}_6$  (\*\*) and  $\text{AlO}_4$  (\*) signals of sillimanite.

perimental line shape (not shown) agrees well with the simulations. The mean quadrupole interaction is stronger for the  $\text{AlO}_4$  tetrahedra, however its distribution width is smaller (below).

The  $^{27}\text{Al}$  NMR line shapes of the various mullites are very complicated and require a careful analysis of the amplitude distribution of the ST spinning sidebands. There are two important points. First, as published previously for a 2/1-type mullite (Kunath-Fandrei et al. 1994a), it is not possible to simulate the intensity distribution of the ST MAS spinning sidebands of the  $\text{AlO}_4$  region using only two  $\text{AlO}_4$  sites [ $\text{AlO}_4(\text{T})$  for the tetrahedra in the double chains and  $\text{AlO}_4(\text{T}^{*s})$  of the triclustered site according to the Sadanaga model]. Only by considering a third  $\text{AlO}_4$  signal is reasonable agreement between experimental and simulated ST MAS line shapes achieved. Hence,  $\text{AlO}_4(\text{T})$ ,  $\text{AlO}_4(\text{T}')$ , and  $\text{AlO}_4(\text{T}^*)$  with isotropic chemical shifts of 69, 55, and 48 ppm, respectively, have been proposed for the assignment of these tetrahedra. Their location in the mullite structure is explained in Figure 1. These signals occur in the spectra of

TABLE 2. NMR parameters

Site	$V'_{zz}$ (MHz)	$\Delta V'_{zz}$ (MHz)	$\eta$	$\Delta\nu$ (kHz)	$\delta_{iso}$ (ppm)	Present in sample
$\text{AlO}_6\text{II}$	0.78(4)	0.42(3)	0.3	1.5	15(1)	GAM, CM2, CM3
$\text{AlO}_4$	0.98(5)	0.32(3)	0.3	2.1	76(1)	GAM, CM2, CM3
$\text{AlO}_6$	0.90(7)	0.50(4)	0.3	0.6	6(1)	CM1, CM2, CM3, FM
$\text{AlO}_4(\text{T})$	1.10(9)	0.55(6)	0	1.5	69(1)	CM1, CM2, FM
	1.10(9)	0.55(6)	0	1.5	71(1)	CM3
$\text{AlO}_4(\text{T}')$	0.90(9)	0.40(3)	0.3	0.9	55(1)	CM1, FM
	1.00(4)	0.50(3)	0.3	0.9	55(1)	CM2
	1.10(8)	0.40(4)	0.3	0.9	60(1)	CM3
$\text{AlO}_4(\text{T}^*)$	0.70(5)	0.40(6)	0.3	0.8	48(1)	CM1
	0.90(9)	0.40(6)	0.5	1.5	46(1)	CM2
	1.00(7)	0.50(3)	0.5	1.5	48(1)	CM3
	0.70(5)	0.40(3)	0.3	1.2	46(1)	FM

Note: This is a summary of the  $^{27}\text{Al}$  quadrupole parameters and isotropic chemical shifts for the various mullites and for the sample GAM ( $\gamma\text{-Al}_2\text{O}_3$ ). For the definition of the mean principal axis value  $V'_{zz}$  of the efg tensor and its distribution width  $\Delta V'_{zz}$  see Experimental section. (Number indicates  $\text{AlO}_6$  in  $\gamma\text{-Al}_2\text{O}_3$ .)

the mullites samples as well. The quadrupole parameters and chemical shifts obtained from the ST MAS sideband analysis are summarized in Table 3. For the Al-rich mullites CM3 and CM2 an additional  $^{27}\text{Al}$  MAS peak is observed at the left shoulder of the  $\text{AlO}_6$  ST MAS lines. It is particularly obvious for CM3. The isotropic chemical shift of 15 ppm is the same as for the  $\text{AlO}_6$  resonance of  $\gamma\text{-Al}_2\text{O}_3$  that is known to be present in these samples by XRD.

The line deconvolution of the NMR spectra (CT region and few ST MAS lines) for the mullite CM3 is shown in the Figure 6 as an example. The simulated lines for the mullite are assigned to as A–D, those for  $\gamma\text{-Al}_2\text{O}_3$  by E and F.

The Al occupancy of the various sites can be determined using the simulations of the ST MAS lines. The main reason for using the ST spectra is that the relative  $\text{AlO}_6$  content of  $\gamma\text{-Al}_2\text{O}_3$  (line F) can be obtained easily and that the corresponding tetrahedrally coordinated Al signal (spectrum E) does overlap only with the  $\text{AlO}_4(\text{T})$  signal of the mullite spectrum. From the NMR ST simulations the total relative Al content in  $\gamma\text{-Al}_2\text{O}_3$  is  $(5 \pm 1)\%$  and  $(20 \pm 1)\%$  for CM2 and CM3, respectively. For completeness, the results of fitting the CT MAS patterns are also listed in Table 3. These data support the ST MAS simulations and the average value of the ST and CT data is used for the plots and in the following discussion. Only for mullite CM3 (large amount of  $\gamma\text{-Al}_2\text{O}_3$ ), are the ST data plotted in Figure 7 as well.

The composition of the mullite sample CM2 ( $x = 0.42$ ) is close to the classical limit for the mullite formation at  $x = 0.5$ . According to our data analysis the total amount of  $\text{AlO}_4(\text{T}')$  and  $\text{AlO}_4(\text{T}^*)$  units is with 8.7% and 5.7% slightly higher as for the 3/2-mullite CM1. In mullite CM3 the composition  $x = 0.69$  exceeds the classical limit of  $x = 0.5$  for the mullite formation. Simultaneously, the relative amount of  $\text{AlO}_4(\text{T}')$  and  $\text{AlO}_4(\text{T}^*)$  units (8.3% and 5% for the mean values of CT and ST, or, 9.3% and 6% for ST only) does not change very much compared

with mullite CM2. The major difference is the increased amount of  $\gamma\text{-Al}_2\text{O}_3$ .

### Structural consequences

The investigated mullites have a broad composition range from 60.37 mol%  $\text{Al}_2\text{O}_3$  (sample CM1) up to 81.04 mol% (sample CM3), which is beyond the classical structure limit for mullites. With increasing  $\text{Al}_2\text{O}_3$  content the relative amount of octahedrally coordinated aluminum ( $\text{AlO}_6$ ) decreases gradually. The same applies for the relative amount of Al in the sillimanite-type tetrahedral double chains [ $\text{AlO}_4(\text{T})$ ]. On the other hand the number of triclustered  $\text{AlO}_4$  tetrahedra [ $\text{AlO}_4(\text{T}^*)$  and  $\text{AlO}_4(\text{T}')$ ] increases as shown in Table 3. Subtracting the relative amount of Al in  $\gamma\text{-Al}_2\text{O}_3$  of some of the mullites and considering the fact that the number of  $\text{AlO}_6$  units per unit cell is constant as can be seen by the formula  $\text{Al}_2(\text{Al}_{2+2x}\text{Si}_{2-2x})\text{O}_{10-x}$  (where Al outside the parentheses = octahedrally coordinated aluminum, Al and Si inside the parentheses = tetrahedrally bonded aluminum and silicon) the occupancy of the various polyhedra can easily be calculated from the data of Table 3. The relative distribution of Al on the various tetrahedrally coordinated sites  $\text{AlO}_4(\text{T}, \text{T}', \text{T}^*)$  vs. the total amount of the  $\text{AlO}_4$  units [ $\sum [^{27}\text{Al}] = \text{AlO}_4(\text{T}) + \text{AlO}_4(\text{T}^*) + \text{AlO}_4(\text{T}')$ ] is plotted in Figure 7 as function of the  $\text{Al}_2\text{O}_3$  content. It turns out that the number of aluminum in the sillimanite type tetrahedra double chains [ $\text{AlO}_4(\text{T})$ ] decreases with the increasing  $\text{Al}_2\text{O}_3$  content accompanied with a corresponding increase of triclustered aluminum [ $\text{AlO}_4(\text{T}^*)$ ] and [ $\text{AlO}_4(\text{T}')$ ] as to be expected.

Figures 7 and 8 compare our experimental findings with the average structure model of mullite [ $\text{Al}_2(\text{Al}_{2+2x}\text{Si}_{2-2x})\text{O}_{10-x}$ , SG = Pbam (55),  $a \approx 7.55 \text{ \AA}$ ,  $b \approx 7.69 \text{ \AA}$ ,  $c \approx 2.88 \text{ \AA}$ ,  $Z = 1$ ], refined and described by Sadanaga et al. (1962) (refinement with  $x = 0.4$ ), Durovic and Fejdi (1976) (Ge mullite with  $x = 0.264$ ), Angel and Prewitt (1986) ( $x = 0.38$ ) using single-crystal X-ray diffraction, and by Angel et al. (1991) (two refinements with

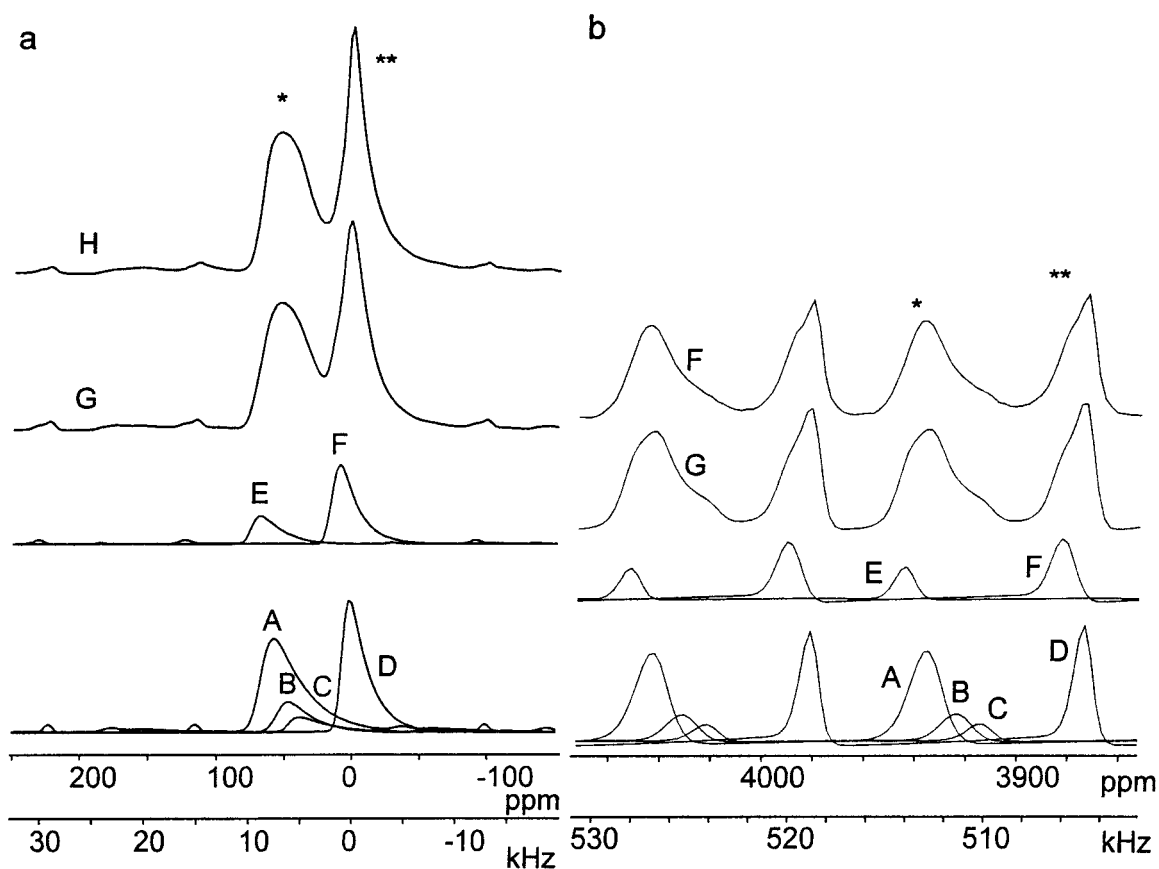


**FIGURE 6.** Comparison of the experimental (H) and simulated (G)  $^{27}\text{Al}$  MAS line shapes of the mullite CM3 for the CT pattern (a) and several ST MAS sidebands (b). According to the line shape analysis a small amount of  $\gamma\text{-Al}_2\text{O}_3$  (E,F) is present. Traces A–D show the simulated spectra for the  $\text{AlO}_4(\text{T})$ ,  $\text{AlO}_4(\text{T}')$ ,  $\text{AlO}_4(\text{T}^*)$ , and the  $\text{AlO}_6$  units of the mullite, respectively. Single star = the fourfold coordination of Al. Double star = the  $\text{AlO}_6$  site. NMR parameters are in Table 3.

$x = 0.4$  fixed, and  $x = 0.386$  refined) using neutron diffraction on a single crystal from the same batch as in their X-ray work.

In the average structure model (Sadanaga et al. 1962), two Al atoms fully occupy the octahedral site O, and two Al atoms sit in the tetrahedral site  $\text{AlO}_4(\text{T})$  with a fixed site occupancy of 0.5. All Al atoms in excess of four in the structure formula,  $\text{Al}_{2,x}$ , occupy exclusively the structurally different tetrahedral site  $\text{AlO}_4(\text{T}^{*s})$ . The Si atoms are assumed to be in the tetrahedral site T only. With the boundary conditions of the Sadanaga model, excellent  $R$  values were obtained in refining single-crystal X-ray data

[(Saalfeld and Guse 1981), 3/2 mullite with  $x = 0.272$ ] or powder X-ray data using the Rietveld method [e.g., Ban and Okada 1992], mullites in the range  $0.262 \leq x \leq 0.492$ . However, in these refinements of X-ray data, due to the similar scattering factors for Si and Al, no distinction of these atoms in the tetrahedral sites T and  $\text{T}^{*s}$  could be made.

In Figure 8 the normalized Al contents of the octahedrally coordinated Al atoms ( $\text{AlO}_6/\Sigma\text{Al}$  with  $\Sigma\text{Al}$  = total Al content in the unit cell) and of all tetrahedrally coordinated Al atoms ( $\Sigma^{[4]}\text{Al}/\Sigma\text{Al}$ ) are shown as a function of the structural state  $x$ . In this plot, variations of the Al/Si

**TABLE 3.** Al occupancy of mullites from NMR analysis

Sample:	CM1		FM		CM2		CM3	
Method:	CT	ST	CT	ST	CT	ST	CT	ST
$\text{AlO}_6$	42.5(3.0)	44(3)	40.3(3.0)	43(3)	39.6(3.0)	37(2)	30.1(3.0)	28(3)
$\text{AlO}_4(\text{T})$	50(3)	50(3)	45.4(3.0)	44(3)	42.1(3.0)	42(3)	37.5(3.0)	36.5(3.0)
$\text{AlO}_4(\text{T}')$	4.8(1.5)	3.7(1.5)	9.9(1.5)	7.6(1.5)	9.5(1.5)	8(1.5)	7.2(1.5)	9.3(1.5)
$\text{AlO}_4(\text{T}^*)$	2.7(1.0)	2.3(1.0)	4.4(1.0)	5.1(1.5)	4.4(1.0)	7(1.5)	3.9(1.5)	6(1.5)

Note: The relative Al content of  $\gamma\text{-Al}_2\text{O}_3$  (ca. 5% and 20% for CM2 and CM3) has been subtracted. For details see text.

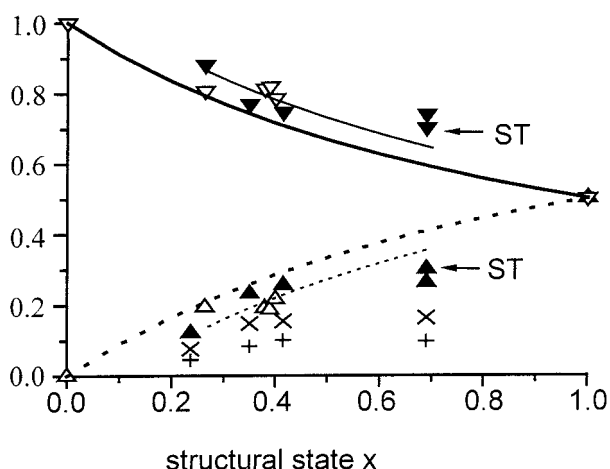


**FIGURE 7.** Al occupancy of the different tetrahedral sites T, T\*, T', and (T\*+T') normalized to all tetrahedrally coordinated Al atoms in the unit cell. Filled symbols = average of CT and ST NMR results; downward pointing triangle =  $\text{AlO}_4(\text{T})/\Sigma^{[4]}\text{Al}$ ; plus sign =  $\text{AlO}_4(\text{T}^*)/\Sigma^{[4]}\text{Al}$ ;  $x = \text{AlO}_4(\text{T}')/\Sigma^{[4]}\text{Al}$ ; upward pointing triangle =  $[\text{AlO}_4(\text{T}^*) + \text{AlO}_4(\text{T}')] / \Sigma^{[4]}\text{Al}$ . Open downward and upward pointing triangles = XRD and neutron diffraction average structure refinements, respectively. Thick curves = average structure model of Sadanaga (T and T\*, respectively). Thin curves = fit of NMR data assuming an Al occupation of the site T of  $0.5 + d$ ,  $d = 0.046(8)$ . ST indicates use of satellite values for sample CM3.

occupation in the different tetrahedral sites are not relevant, because the total Al contents of the octahedra and the tetrahedra are calculated. The curves and open symbols correspond to the average structure model of Sadanaga [octahedrally coordinated Al =  $1/(2+x)$ ; tetrahedrally coordinated Al =  $(1+x)/(2+x)$ ] and to the structure refinements from the other above-cited literature, respectively. The filled symbols are the values obtained in this NMR study. It is evident that the relative Al content of the octahedral and of all tetrahedral sites together agrees well with the average structure model. In the literature, the full occupation of the chains of octahedra,  $(\text{Al}_2\text{O}_8)^{-10}$ , is undoubtedly assumed to be the case even for the real structure of mullite, which represents a complex, partially disordered, incommensurate, superlattice structure [see e.g., Schneider et al. (1994a)]. Our NMR results support this model and could also be regarded as a confidence test of the NMR method itself.

Because whether T\* is occupied by Al atoms alone or in combination with Si (or Ge) atoms, still is of outstanding interest, we focus now on the distribution of the tetrahedrally coordinated atoms in the structure  $[(\text{Al}_{2+2x}\text{Si}_{2-2x})\text{O}_{2-x}]^{10+}$ . Several attempts have been made previously to solve this question using classical diffraction methods. Durovic and Fejdi (1976) analyzed an isostructural Ge mullite, where a considerable difference between atomic numbers of Al and Ge gives a better chance to distinguish these atoms. Angel and Prewitt (1986) refined single-crystal X-ray data of a Si mullite taking into

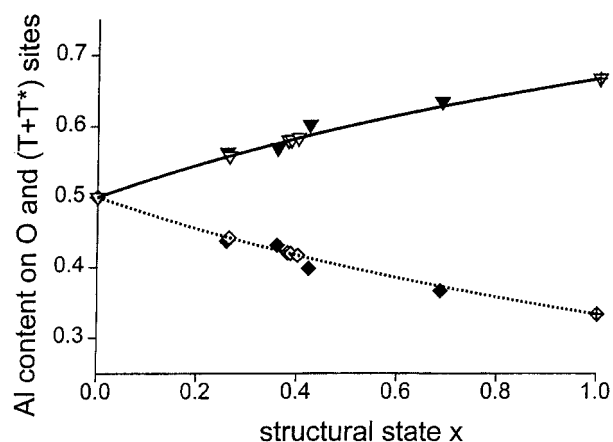


**FIGURE 8.** Octahedrally and tetrahedrally coordinated Al atoms normalized to the total Al content of the unit cell ( $\Sigma\text{Al}$ ) of mullite. Solid and dotted curves = structure model of Sadanaga. Filled diamonds =  $\text{AlO}_6/\Sigma\text{Al}$ ; filled triangles =  $\Sigma^{[4]}\text{Al}/\Sigma\text{Al}$ ; both are NMR results. Open diamonds = XRD; open triangles = neutron diffraction, both are average structure refinements.

account anharmonic temperature factors (third- and fourth-rank tensors) for the fully occupied O sites, varying occupancies for the partially occupied O sites, and varying Al/Si occupancies for both T and T\*s sites. Finally, Angel et al. (1991) refined single-crystal neutron diffraction data, where significant differences of the neutron cross sections between Al and Si occur. In Figure 7 (upward pointing filled triangles) the Al content of the sites T\* and T' of this NMR study were added together to make our results comparable to the refined average structures. This sum corresponds to T\*s as explained earlier. Only for mullite CM3 the ST value is shown additionally, for the reasons mentioned earlier in the  $^{27}\text{Al}$  line shape discussion. In our view this value is more reliable than the CT result. Hence it has been used for the following calculations.

The NMR results obviously indicate that the T site exhibits a somewhat higher Al occupation, and consequently the T\* site a somewhat lower, than in the simple structure model of Sadanaga. In the composition region of the analyzed samples  $2.5 \leq x \leq 0.7$  the NMR data points for the Al occupancy on the T site were fitted to the function  $(1 + 2d)/(1 + x)$  (thin curves in Fig. 7) and a constant occupancy deviation from the Sadanaga model was found [ $d = 0.046(8)$ , least square standard deviation is given in parenthesis]. Instead of a fixed Al site occupancy of 0.5, according to the Sadanaga model, the more likely occupancy is  $0.5 + d = 0.546(8)$ , according to our NMR data. This result agrees well with X-ray and neutron structure refinements by Angel and Prewitt ( $x = 0.38$ ,  $d = 0.06$ , and  $x = 0.386$ ,  $d = 0.065$ , and  $x = 0.40$ ,  $d = 0.05$ ), but differs clearly from the data published by Durovic and Fejdi for a Ge mullite ( $x = 0.264$ ,  $d = 0.01$ ). However, all those authors note, that in their refinements the R values were not sensitive against variations of the Al/Si (or Ge) occupancies in the tetrahedral sites T and T\*s. Thus,

the *R* values alone cannot be used to decide which occupancy relation is correct. Furthermore, because an average structure represents a space and time projection of the long-range ordered and disordered real structure, the question arises of how physically realistic thermal motions of atoms modify the X-ray diffraction patterns of a crystal having superlattice, satellite, and diffuse scattered intensities. This is why Angel and Prewitt recommended using NMR as an alternative method for solving the problem of tetrahedral site occupancies in mullite.

### Conclusion

This study shows that NMR is a powerful tool to study the coordination spheres and occupancies in crystalline solids with complex translation symmetry, where the classical, successful methods of structure determination cannot solve all structural questions. Particularly, the relative Al occupancy of the various sites can be measured using powder samples instead of single crystals. The recent progress is based on a careful analysis of the  $^{27}\text{Al}$  ST MAS spinning sidebands. This yields reliable data of the relevant quadrupole parameters, which in turn were used to fit the CT MAS patterns such that the relative  $^{27}\text{Al}$  occupancy can be determined both by the CT and ST MAS line shape analyses.

### ACKNOWLEDGMENT

Financial support by the Deutsche Forschungsgemeinschaft is gratefully acknowledged.

### REFERENCES CITED

- Alemany, L.B., Massiot, D., Sherriff, B.L., Smith, M.E., and Taulelle, F. (1991) Observation and accurate quantification of  $^{27}\text{Al}$  MAS NMR spectra of some  $\text{Al}_2\text{SiO}_5$  polymorphs containing sites with large quadrupole interactions. *Chemical Physics Letters*, 177, 301–306.
- Angel, R.J. and Prewitt, C.T. (1986) Crystal structure of mullite: A re-examination of the average structure. *American Mineralogist*, 71, 1476–1482.
- Angel, R.J., McMullan, R.K., and Prewitt, C.T. (1991) Substructure and superstructure of mullite by neutron diffraction. *American Mineralogist*, 76, 332–342.
- Ban, T. and Okada, K. (1992) Structure refinement of mullite by the Rietveld method and a new method for estimation of chemical composition. *Journal of the American Ceramic Society*, 75, 227–230.
- Bauchspiess, K.R. (1995) EXAFS background subtraction using splines. *Physica B*, 208–209, 185–186.
- Bish, D.L. and Burnham, C.W. (1992) Rietveld refinement of the crystal structure of fibrolitic sillimanite using neutron powder diffraction data. *American Mineralogist*, 77, 374–379.
- Boch, P., Chartier, T., and Rodrigo, P.D.D. (1990) High-purity mullite ceramics by reaction sintering. *Ceramic Transactions*, 6, 353–374.
- Brindley, G.W. and Nakahira, M. (1959a) The kaolinite-mullite reaction series: I. Survey of outstanding problems. *Journal of the American Ceramic Society*, 42, 311–314.
- (1959b) The kaolinite-mullite reaction series: II. Metakaolin. *Journal of the American Ceramic Society*, 42, 314–318.
- (1959c) The kaolinite-mullite reaction series: III. The high-temperature phases. *Journal of the American Ceramic Society*, 42, 319–324.
- Burnham, C.W. (1963) The crystal structure of mullite. *Carnegie Institution of Washington Year Book*, 62, 158–165.
- (1964a) Crystal structure of mullite. *Carnegie Institution of Washington Year Book*, 63, 223–227.
- (1964b) Composition limits of mullite, and the sillimanite-mullite solid solution problem. *Carnegie Institution of Washington Year Book*, 63, 227–228.
- Cameron, W.E. (1977a) Mullite: a substituted alumina. *American Mineralogist*, 62, 747–755.
- (1977b) Composition and cell dimensions of mullite. *Bulletin of the American Ceramic Society*, 56, 1003–1011.
- Davies, T.J., Emblem, H.G., and Jones, K. (1990) Preparation and Properties of Mullite Grain. *British Ceramic Transactions and Journal*, 89, 44–50.
- Durovic, S. (1969) Refinement of crystal structure of mullite. *Chemické Zvesti*, 23, 113–128.
- Durovic, S. and Fejdi, P. (1976) Synthesis and crystal structure of germanium mullite and crystallochemical parameters of D-mullite. *Silikaty*, 2, 97–112.
- Fischer, X.F., Schneider, H., and Schmücker, M. (1994) Crystal structure of Al-rich mullite. *American Mineralogist*, 79, 983–990.
- Fischer, X.F., Schneider, H., and Voll, D. (1996) Formation of Aluminum rich 9:1 mullite and its transformation to low alumina mullite upon heating. *Journal of European Ceramic Society*, 16, 109–113.
- Freude, D. and Haase, J. (1993) Quadrupole effects in solid-state nuclear magnetic resonance. In *NMR-Basic Principles and Progress*; vol 29, 1–90, Springer Verlag, Berlin Heidelberg.
- Jäger, C. (1994) Satellite transition spectroscopy. In *NMR-Basic Principles and Progress*; Vol. 31, 133–170, Springer Verlag, Berlin Heidelberg.
- Jäger, C., Müller-Warmuth, W., Mundus, C., and van Wüllen, L. (1992)  $^{27}\text{Al}$  MAS-NMR spectroscopy of glasses: new facilities by application of 'SATRAS'. *Journal of Non-Crystalline Solids*, 149, 209–217.
- Jäger, C., Kunath, G., Losso, P., and Scheler, G. (1993a) Determination of distributions of the quadrupole interaction in amorphous solids by  $^{27}\text{Al}$  satellite transition spectroscopy. *Solid State Nuclear Magnetic Resonance*, 2, 73–82.
- Jäger, C., Dupree, R., Kohn, S.C., and Mortuza, M.G. (1993b)  $^{17}\text{O}$  satellite transition spectroscopy of amorphous  $\text{SiO}_2$ . *Journal of Non-Crystalline Solids*, 155, 95–98.
- Klug, F.J., Prochazka, S., and Doremus, R.H. (1990) Alumina-silica phase diagram in the mullite region. *Ceramic Transactions*, 6, 15–43.
- Kunath, G., Losso, P., Steuernagel, S., Schneider, H., and Jäger, C. (1992)  $^{27}\text{Al}$  satellite transition spectroscopy (SATRAS) of polycrystalline aluminum borate  $9\text{Al}_2\text{O}_3 \cdot 2\text{B}_2\text{O}_3$ . *Solid State Nuclear Magnetic Resonance*, 1, 261–266.
- Kunath-Fandrei, G., Rehak, P., Steuernagel, S., Schneider, H., and Jäger, C. (1994a) Quantitative structural analysis of mullite by  $^{27}\text{Al}$  NMR satellite spectroscopy. *Solid State Nuclear Magnetic Resonance*, 3, 241–248.
- Kunath-Fandrei, G., Ehrt, D., and Jäger, C. (1994b) Progress in structural elucidation of glasses by  $^{27}\text{Al}$  and  $^{11}\text{B}$  satellite transition NMR spectroscopy. *Zeitschrift für Naturforschung*, 50a, 413–422.
- Kunath-Fandrei, G., Bastow, T.J., Jäger, C., and Smith, M.E. (1995a) Quadrupole and chemical shift interactions of  $^{27}\text{Al}$  in aluminum molybdate from satellite transition magic angle spinning NMR. *Chemical Physics Letters*, 234, 431–438.
- Kunath-Fandrei, G., Bastow, T.J., Hall, J.S., Jäger, C., and Smith, M.E. (1995b) Quantification of aluminum coordinations in amorphous aluminas by combined central and satellite transition NMR spectroscopy. *Journal of Physical Chemistry*, 99, 15138–15141.
- Lippmaa, E., Samoson, A., and Mägi, M. (1986) High resolution  $^{27}\text{Al}$  NMR of aluminosilicates. *Journal of the American Chemical Society*, 106, 1730–1735.
- Merwin, L.H., Sebald, A., Rager, H., and Schneider, H. (1991)  $^{29}\text{Si}$  and  $^{27}\text{Al}$  MAS NMR spectroscopy of mullite. *Physics and Chemistry of Minerals*, 18, 47–52.
- Rager, H., Schneider, H., and Graetsch, H. (1990) Chromium incorporation in mullite. *American Mineralogist*, 75, 392–397.
- Rahman, H.S. and Weichert, H.-T. (1990) Interpretation of HREM images of mullite. *Acta Crystallographica Section B*, Structural, 46, 139–149.
- Raymond, M. and Hafner, S. (1970) Nuclear quadrupole coupling tensors of aluminum-27 in sillimanite ( $\text{Al}_2\text{SiO}_5$ ). *Journal of Chemical Physics*, 53, 4110–4111.
- Saalfeld, H. and Guse, W. (1981) Structure refinement of 3:2 mullite

- $3\text{Al}_2\text{O}_3 \cdot 2\text{SiO}_2$ . Neues Jahrbuch für Mineralogie Monatshefte, 4, 145–150.
- Sadanaga, R., Tokonami, M., and Takeuchi, Y. (1962) The structure of mullite,  $2\text{Al}_2\text{O}_3 \cdot \text{SiO}_2$ , and relationship with that of sillimanite and andalusite. Acta Crystallographica, 15, 65–68.
- Samoson, A. (1985) Satellite transition high-resolution NMR of quadrupolar nuclei in powders. Chemical Physics Letters, 119, 29–32.
- Sanz, J., Madani, A., Serratos, J.M., Moya, J.S., and Aza, S. (1988) Aluminum-27 and silicon-29 magic-angle spinning nuclear magnetic resonance study of the kaolinite-mullite transformation. Journal of the American Ceramic Society, 71, C 418–C 421.
- Sanz, J., Sobrados, I., Cavalieri, A.L., Pena, P., Aza, S., and Moya, J.S. (1991) Structural changes induced on mullite precursors by thermal treatment: a  $^{27}\text{Al}$  MAS-NMR investigation. Journal of the American Ceramic Society, 74, 2398–2403.
- Schmucker, M., Albers, W., and Schneider, H. (1994) Mullite formation by reaction sintering of quartz and  $\alpha$ -alumina—a TEM study, Journal of the European Ceramic Society, 14, 511–515.
- Schneider, H., Merwin, L., and Sebald, A. (1992) Mullite formation from non-crystalline precursors. Journal of Materials Science, 27, 805–812.
- Schneider, H., Fischer, R.X., and Voll, D. (1993) Mullite with Lattice Constants  $a > b$ . Journal of the American Ceramic Society, 76, 1879–1886.
- Schneider, H., Okada, K., and Pask, J.A. (1994a) Mullite and mullite ceramics. Wiley, Chichester.
- Schneider, H., Voll, D., and Mosset, A. (1994b) Synthesis and structural characterization of non-crystalline mullite precursors. Journal of Non-Crystalline Solids, 178, 262–269.
- Skibsted, J., Nielsen, N.C., Bildsoe, H., and Jakobsen, H.J. (1991) Satellite transitions in MAS NMR spectra of quadrupolar nuclei. Journal of Magnetic Resonance, 95, 88–117.
- Smith, M.E. (1993) Application of aluminum-27 NMR techniques to structure determination in solids. Applied Magnetic Resonance, 4, 1–64.
- Smith, M.E., Jäger, C., Schönhofer, R., and Steuernagel, S. (1994) Structural characterization of the aluminum sites in kyanite by  $^{27}\text{Al}$  magic angle spinning centreband, satellite transition and double rotation NMR. Chemical Physics Letters, 219, 75–80.
- Somiya, S., Davies, R.F., and Pask, J.A. Eds. (1990) Mullite and Mullite Matrix Composites. Ceramic Transactions, 6, 1–9.
- Taylor, A. and Holland, D. (1993) The chemical synthesis and crystallization sequence of mullite. Journal of Non-Crystalline Solids, 152, 1–17.
- Voll, D. (1995) Mullitprecursoren: Synthese, temperaturabhängige Entwicklung der strukturellen Ordnung und Kristallisationsverhalten. in: Fortschritt-Berichte VDI, Reihe 5, Grund- und Werkstoffe Nr. 411, VDI Verlag, Düsseldorf.

MANUSCRIPT RECEIVED JULY 22, 1997

MANUSCRIPT ACCEPTED JUNE 8, 1998

PAPER HANDLED BY JONATHAN F. STEBBINS